

Computational investigation of the effect of α -alkylation on S_N2 reactivity: acid-catalyzed hydrolysis of alcohols

2 PERKIN

Giuseppe D. Ruggiero and Ian H. Williams*

Department of Chemistry, University of Bath, Bath, UK BA2 7AY.

E-mail: i.h.williams@bath.ac.uk

Received (in Cambridge, UK) 2nd January 2001, Accepted 25th January 2001

First published as an Advance Article on the web 20th February 2001

Computed potential energy barriers (HF, B3LYP and MP2/6-31G*; vacuum and PCM water) for simple S_N2 identity reactions $H_2O + R-OH_2^+ \rightarrow ^+H_2O-R + OH_2$ tend to decrease along the series $R = Me, Et, Pr^i$ and Bu^t , in contrast with those calculated for $Cl^- + R-Cl \rightarrow Cl-R + Cl^-$. The S_N2 reaction profile for $H_2O + Bu^t-OH_2^+$ shows a sequence of three steps, each with a transition structure corresponding to the internal rotation of a single methyl substituent. The same three rotations also appear in the S_N2 reaction profile for $Cl^- + Bu^t-Cl$, but as distinct stages of a concerted process with a single transition structure; only the second methyl group undergoes internal rotation in the transition vector itself. Simulation of reactions $H_2O + R-OH_2^+$, using the AM1/COSMO method for treatment of aqueous solvation, illustrates the changing energy surface topography accompanying S_N2/S_N1 mechanistic changeover along the series $R = Me, Et, Pr^i$ and Bu^t , and permits determination of kinetic isotope effects for *both* pathways with *each* alkyl group. Mechanistic change occurs by alteration of the relative energies of the TSs along these competing paths. Computational modelling allows investigation of experimentally unobserved reaction mechanisms, such as S_N1 for primary substrates.

Introduction

Every student of organic chemistry learns that the relative rate of bimolecular nucleophilic substitution [eqn. (1)] decreases



along the series $R = Me, Et, Pr^i, Bu^t$, as a consequence of increasing steric hindrance between the nucleophile X^- and the methyl substituents attached to the α -carbon of the electrophile $R-Y$. The evidence to support this fact originates from the classic experiments of Ingold and co-workers¹ where X and Y are halogens and, of course, the reacting system bears a negative charge overall. While the quantitative accuracy of the data for the S_N2 reaction with $R = Bu^t$ has been criticized,² the qualitative veracity of the reactivity trend $Me > Et > Pr^i > Bu^t$ remains unchallenged.

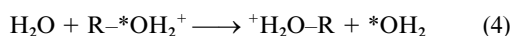
Does the same trend hold for S_N2 reactions [eqn. (2)] between



a neutral nucleophile Nu and a cationic electrophile $R-Z^+$? We are unaware that any systematic series of experiments has been reported in the literature for bimolecular nucleophilic substitutions of this type with $R = Me, Et, Pr^i, Bu^t$. A simple example would be the identity reaction of water with a protonated alcohol [eqn. (3)], observable by isotopic substitution.³

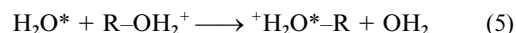


McClelland has measured rate constants for isotopic exchange of ^{18}O -labelled methanol in acidic media [eqn. (4), $R = Me$] and



has shown that this reaction proceeds by the S_N2 mechanism, but that the corresponding reaction of *tert*-butyl alcohol takes place by an S_N1 mechanism.⁴

Uggerud and Bache-Andreassen recently studied⁵ these reactions [eqn. (5), $R = Me, Et, Pr^i, Bu^t$] at low pressure by



means of ion cyclotron resonance mass spectrometry, and determined the relative rate constants to be approximately 1 : 0.3 : 200 : 2000. They also obtained this order of gas-phase reactivity from MP2 and B3LYP calculations of backside S_N2 barrier heights using the 6-31G(d) basis.⁵ Their results suggest that the effect of α -alkylation upon S_N2 reactivity may not necessarily be the same for cationic systems as for anionic ones.

In this paper we present the results of electronic structure calculations for S_N2 reactions of water with protonated alcohols *in vacuo* and within a dielectric continuum to represent the effect of aqueous solvation. First, we investigate the effect of α -alkylation, contrasting our results with those for the reaction of chloride anion with chloroalkanes. Second, we consider the detailed reaction path for these backside nucleophilic substitutions, with particular emphasis upon the timing of the methyl-group rotations for the case of $R = Bu^t$. Third, we explore the manner of the S_N2/S_N1 mechanistic changeover in nucleophilic aliphatic substitution. Fourth, we present calculated kinetic isotope effects for these reactions proceeding by both unimolecular and bimolecular mechanisms.

Computational methods

The Gaussian 98 program⁶ was employed with the 6-31G* basis for HF and B3LYP geometry optimization both *in vacuo* and with the polarized continuum model (PCM)⁷ for aqueous solvation, and for MP2 geometry optimization *in vacuo* and single-point PCM/MP2 energies at MP2 geometries. The MOPAC93 program⁸ was used for semiempirical AM1 calculations *in vacuo* and with the conductor-like screening model (COSMO) for aqueous solvation.⁹ Transition structures (TSs) were located by means of the EF algorithm and characterized by frequency calculations, both *in vacuo* and in water, and by

intrinsic reaction co-ordinate calculations to verify the adjacent local minima. Unless stated, no symmetry constraints were imposed. The 6-31G* basis was used throughout, even for anionic systems, in order to achieve comparability with previously published work.

Kinetic isotope effects (KIEs) at 298.15 K were evaluated from the optimized geometries and computed force constants using our CAMISO program.¹⁰ Unwanted contamination of the Hessians by spurious translational and rotational contributions was eliminated by a projection method to yield pure vibrational frequencies. Partition functions were evaluated within the harmonic-oscillator, rigid-rotor, ideal-gas approximations and were utilized within a standard semi-classical transition-state theoretical treatment of isotope effects.¹¹

Results and discussion

Tables 1 and 2 contain total and relative energies for geometry-optimized separated reactants, reactant complexes (RCs) and TSs for both $\text{Cl}^- + \text{RCl}$ and $\text{H}_2\text{O} + \text{R-OH}_2^+$ identity reactions with $\text{R} = \text{Me, Et, Pr}^i$ and Bu' , along with transition frequencies for all TSs. The relative energies are the potential energy barriers calculated with respect to either the separated species (ΔE_r^\ddagger) or the reactant complex (ΔE_{rc}^\ddagger). Tables 3 and 4 contain optimized bond lengths for the bonds between the α -carbon atom and the nucleophile and the leaving group for the same $\text{Cl}^- + \text{RCl}$ and $\text{H}_2\text{O} + \text{R-OH}_2^+$ species. Tables 5 and 6 contain Pauling bond orders¹² and tightness parameters for RCs and TSs for the two series of reactions. The Pauling bond order $n(\text{C}\cdots\text{X})$ for a $\text{C}\cdots\text{X}$ bond is given by $n(\text{C}\cdots\text{X}) = \exp[(r_1 - r_n)/c]$. Here r_1 and r_n are bond lengths for $\text{C}\cdots\text{X}$ bonds of order 1.0 and n , respectively. Although a value of 0.3

for the coefficient c has been widely employed, we have noted elsewhere that, as this value correlates to changes in bond order > 1 , due largely to changes in the degree of π -bonding, a different value is more appropriate for changes in bond order < 1 , which are largely due to changes in the degree of σ -bonding.¹³ We determine the value of c for each theoretical method by defining the $\text{C}\cdots\text{X}$ bond in the $\text{S}_{\text{N}}2$ TS involving MeX to have $n = 0.5$.¹⁴ Tightness parameters τ^{RC} and τ^{TS} may be defined,¹⁴ following Albery and Kreevoy,¹⁵ as $\tau^{\text{RC}} = n(\text{C}\cdots\text{X}_{\text{nuc}})^{\text{RC}} + n(\text{C}\cdots\text{X}_{\text{lg}})^{\text{RC}}$ and $\tau^{\text{TS}} = n(\text{C}\cdots\text{X}_{\text{nuc}})^{\text{TS}} + n(\text{C}\cdots\text{X}_{\text{lg}})^{\text{TS}}$, and their difference as $\Delta\tau^\ddagger = \tau^{\text{TS}} - \tau^{\text{RC}}$.

Effect of α -alkylation on $\text{S}_{\text{N}}2$ reactivity

The upper part of Fig. 1 shows barrier heights calculated for the $\text{Cl}^- + \text{RCl}$ identity reactions in a vacuum and in water. Our MP2/6-31G* results *in vacuo* agree essentially with those reported by Jensen,¹⁶ with one difference of detail as noted in the next section. In particular, the HF, B3LYP and MP2 methods all show that the barrier to reaction, either ΔE_r^\ddagger or ΔE_{rc}^\ddagger , increases along the series $\text{R} = \text{Me, Et, Pr}^i, \text{Bu}'$ in accordance with expectation. The energy barriers ΔE_r^\ddagger are all lower than the values of ΔE_{rc}^\ddagger by the amount of the energy of association ΔE_{assoc} of the ion-molecule RC, a negative quantity: $\Delta E_r^\ddagger = \Delta E_{rc}^\ddagger + \Delta E_{\text{assoc}}$. The calculated values of ΔE_{assoc} for association of Cl^- with MeCl *in vacuo* (HF, -42.8 ; B3LYP, -49.7 ; MP2, -45.5 kJ mol^{-1}) are in good agreement with experiment¹⁷ (-43.5 kJ mol^{-1} at 298 K). The HF and MP2 values of ΔE_r^\ddagger calculated for the $\text{Cl}^- + \text{MeCl}$ identity reaction *in vacuo* (15.5 and 19.0 kJ mol^{-1} , respectively) agree reasonably with experiment¹⁸ (10.5 kJ mol^{-1} at 298 K). However, B3LYP predicts a negative value of ΔE_r^\ddagger (-21.5 kJ mol^{-1})

Table 1 Total energies (hartree), relative energies and transition frequencies for optimized structures for $\text{Cl}^- + \text{R-Cl}$

	Vacuum			Water		
	HF	B3LYP	MP2	PCM/HF	PCM/B3LYP	PCM/MP2 ^a
Cl^-	-459.52600	-460.25223	-459.65210	-459.65229	-460.37860	-459.77834
R = Me						
RCl	-499.09315	-500.10914	-499.35456	-499.09424	-500.10854	-499.35499
$\text{Cl}^- \cdots \text{RCl}$	-958.63550	-960.38032	-959.02401	-958.73433	-960.47685	-959.12895
TS	-958.61346	-960.36958	-958.99943	-958.69970	-960.45249	-959.08319
ν^*/cm^{-1}	415i	327i	510i	469i	415i	—
$\Delta E_r^\ddagger/\text{kJ mol}^{-1}$	15.0	-21.5	19.0	122.9	90.9	131.6
$\Delta E_{rc}^\ddagger/\text{kJ mol}^{-1}$	57.8	28.2	64.5	90.9	63.9	120.1
R = Et						
RCl	-538.13152	-539.42836	-538.52402	-538.13401	-539.42627	-538.52546
$\text{Cl}^- \cdots \text{RCl}$	-997.67514	-999.69944	-998.19598	-997.77293	-999.79502	-998.29728
TS	-997.64748	-999.68177	-998.16275	-997.73595	-999.76851	-998.24567
ν^*/cm^{-1}	367i	307i	498i	345i	375i	—
$\Delta E_r^\ddagger/\text{kJ mol}^{-1}$	26.3	-3.1	35.1	132.2	95.5	152.6
$\Delta E_{rc}^\ddagger/\text{kJ mol}^{-1}$	72.6	46.4	87.2	97.1	69.6	135.5
R = Prⁱ						
RCl	-577.16936	-578.74607	-577.69515	-577.17223	-578.74360	-577.69666
$\text{Cl}^- \cdots \text{RCl}$	-1036.71444	-1039.01943	-1037.36955	-1036.79904	-1039.10544	-1037.46687
TS	-1036.68353	-1038.99503	-1037.32877	-1036.77195	-1039.07848	-1037.41133
ν^*/cm^{-1}	320i	307i	492i	266i	331i	—
$\Delta E_r^\ddagger/\text{kJ mol}^{-1}$	31.1	8.6	48.5	138.0	114.7	167.1
$\Delta E_{rc}^\ddagger/\text{kJ mol}^{-1}$	81.1	64.0	107.1	71.1	70.8	145.8
R = Bu'						
RCl	-616.20588	-618.06173	-616.86725	-616.20846	-618.06182	-616.86830
$\text{Cl}^- \cdots \text{RCl}$	-1075.75273	-1078.33855	-1076.54493	-1075.83241	-1078.42580	-1076.63810
TS	-1075.71687	-1078.29988	-1076.48419	-1075.81019	-1078.38248	-1076.56605
ν^*/cm^{-1}	213i	278i	431i	167i	307i	—
$\Delta E_r^\ddagger/\text{kJ mol}^{-1}$	39.4	37.0	92.3	132.7	152.1	211.6
$\Delta E_{rc}^\ddagger/\text{kJ mol}^{-1}$	94.1	101.5	159.5	58.3	113.7	189.1

^a Single-point PCM/MP2/6-31G**//MP2/6-31G* energies.

Table 2 Total energies (hartree), relative energies and transition frequencies for optimized structures for H₂O + R–OH₂⁺

	Vacuum			Water		
	HF	B3LYP	MP2	PCM/HF	PCM/B3LYP	PCM/MP2 ^a
H ₂ O	-76.01075	-76.40895	-76.19685	-76.02143	-76.41707	-76.20723
R = Me						
ROH ₂ ⁺	-115.33899	-116.01574	-115.64585	-115.48092	-116.15840	-115.78703
H ₂ O⋯ROH ₂ ⁺	-191.36893	-192.44527	-191.86391	-191.50435	-192.58137	-192.00482
TS	-191.35432	-192.43482	-191.84683	-191.45593	-192.54177	-191.95109
$\nu^{\ddagger}/\text{cm}^{-1}$	370i	363i	499i	500i	451i	—
$\Delta E_r^{\ddagger}/\text{kJ mol}^{-1}$	-12.1	-26.6	-10.8	121.8	88.4	113.3
$\Delta E_{rc}^{\ddagger}/\text{kJ mol}^{-1}$	38.4	27.4	44.8	127.1	103.9	141.1
R = Et						
ROH ₂ ⁺	-154.38716	-155.34446	-154.82424	-154.52223	-155.48143	-154.95829
H ₂ O⋯ROH ₂ ⁺	-230.41553	-231.77238	-231.04167	-230.54067	-231.89857	-231.17597
TS	-230.40304	-231.75865	-231.02069	-230.49941	-231.86229	-231.12079
$\nu^{\ddagger}/\text{cm}^{-1}$	199i	311i	427i	347i	375i	—
$\Delta E_r^{\ddagger}/\text{kJ mol}^{-1}$	-13.5	-13.7	1.0	116.2	95.1	117.4
$\Delta E_{rc}^{\ddagger}/\text{kJ mol}^{-1}$	32.8	36.0	55.1	108.3	95.3	144.8
R = Pr ⁱ						
ROH ₂ ⁺	-193.43385	-194.67146	-194.00207	-193.55845	-194.79820	-194.12643
H ₂ O⋯ROH ₂ ⁺	-269.46126	-271.09857	-270.21859	-269.58310	-271.21658	-270.34450
TS	-269.45483	-271.08495	-270.19922	-269.54459	-271.18086	-270.29116
Int	-269.45487					
$\nu^{\ddagger}/\text{cm}^{-1}$	117i	261i	296i	216i	332i	—
$\Delta E_r^{\ddagger}/\text{kJ mol}^{-1}$	-25.8	-12.0	-0.8	92.6	90.3	111.6
$\Delta E_{rc}^{\ddagger}/\text{kJ mol}^{-1}$	17.9	35.8	50.9	101.1	93.8	140.0
R = Bu ^f						
ROH ₂ ⁺	-232.47816	-233.99380	-233.18169	-232.59286	-234.10819	-233.29462
H ₂ O⋯ROH ₂ ⁺	-308.50687	-310.42328	-309.39761	-308.61766	-310.53288	-309.51613
TS ₁	-308.50650	-310.41670	-309.38387	-308.58676	-310.49917	-309.46434
$\nu_1^{\ddagger}/\text{cm}^{-1}$	109i	95i	99i	114i	126i	—
Int	-308.50693	-310.41678	-309.38391	-308.58720	-310.50176	-309.46391
TS ₂	-308.50613	-310.41496	-309.38244	-308.58702	-310.49755	-309.46273
$\nu_2^{\ddagger}/\text{cm}^{-1}$	136i	157i	167i	142i	195i	—
$\Delta E_r^{\ddagger}/\text{kJ mol}^{-1}$	-45.2	-32.0	-10.3	71.6	67.4	102.7
$\Delta E_{rc}^{\ddagger}/\text{kJ mol}^{-1}$	1.9	21.8	39.8	80.4	92.7	140.2

^a Single-point PCM/MP2/6-31G**//MP2/6-31G* energies.**Table 3** Optimized bond lengths (Å) for structures along the reaction path for Cl⁻ + R–Cl

	Vacuum				Water					
	HF		B3LYP		MP2		PCM/HF		PCM/B3LYP	
R = Me	C⋯Cl _{nuc}	C⋯Cl _{lg}								
RCl		1.784		1.809		1.791		1.791		1.803
Cl ⁻ ⋯RCl	3.266	1.828	3.085	1.871	3.161	1.814	3.306	1.806	3.199	1.829
TS	2.383	2.382	2.364	2.363	2.309	2.308	2.388	2.387	2.348	2.346
R = Et		1.799		1.834		1.799		1.812		1.822
RCl		1.840	3.369	1.870	3.351	1.814	3.486	1.825	3.369	1.848
Cl ⁻ ⋯RCl	3.453	2.468	2.463	2.395	2.370	2.344	2.528	2.500	2.449	2.422
TS	2.477									
R = Pr ⁱ		1.815		1.859		1.815		1.832		1.842
RCl		1.856	3.608	1.889	3.740	1.832	3.525	1.838	3.774	1.866
Cl ⁻ ⋯RCl	3.726	2.589	2.518	2.518	2.422	2.422	2.684	2.667	2.559	2.541
TS	2.590									
R = Bu ^f		1.834		1.884		1.834		1.854		1.882
RCl		1.869	3.685	1.919	3.849	1.848	3.687	1.873	4.173	1.896
Cl ⁻ ⋯RCl	4.351	2.982	2.767	2.767	2.642	2.608	3.134	3.129	2.915	2.915
TS	2.984									

in common with many DFT methods.¹⁹ To obtain near-quantitative agreement for the barrier height²⁰ requires a much larger basis set and a much better treatment of electron correlation energy than has been used here; calculations at, say, the

G2 level of theory would not be feasible for the larger alkyl groups considered in this work. Our MP2 calculated values of ΔE_{assoc} for association of Cl⁻ with EtCl, PrⁱCl, and Bu^fCl *in vacuo* agree with experiment¹⁷ to within ± 3 kJ mol⁻¹.

Table 4 Optimized bond lengths (Å) for structures along the reaction path for H₂O + R-OH₂⁺

	Vacuum						Water			
	HF		B3LYP		MP2		PCM/HF		PCM/B3LYP	
R = Me	C···O _{nuc}	C···O _{lg}								
ROH ₂ ⁺		1.511		1.521		1.511		1.511		1.521
H ₂ O···ROH ₂ ⁺	2.695	1.537	2.603	1.554	2.622	1.542	2.695	1.537	2.603	1.554
TS	2.039	2.039	1.975	1.974	1.953	1.953	2.003	2.003	1.959	1.958
R = Et										
ROH ₂ ⁺		1.546		1.567		1.547		1.546		1.569
H ₂ O···ROH ₂ ⁺	2.874	1.572	2.825	1.590	3.195	1.567	2.874	1.572	2.825	1.590
TS	2.208	2.208	2.094	2.094	2.061	2.060	2.134	2.134	2.044	2.043
R = Pr ⁱ										
ROH ₂ ⁺		1.591		1.619		1.580		1.591		1.619
H ₂ O···ROH ₂ ⁺	3.028	1.617	2.945	1.638	3.372	1.594	3.028	1.617	2.945	1.619
TS	2.511	2.376	2.261	2.261	2.249	2.249	2.315	2.315	2.168	2.168
Int	2.462	2.462								
R = 'Bu										
ROH ₂ ⁺		1.664		1.642		1.602		1.664		1.645
H ₂ O···ROH ₂ ⁺	3.482	1.744	3.392	1.724	3.419	1.627	3.482	1.744	3.392	1.724
TS ₁	3.077	2.515	3.216	2.429	2.976	2.421	2.919	2.380	3.216	2.427
Int	2.957	2.647	3.215	2.548	2.941	2.475	2.861	2.471	2.889	2.467
TS ₂	2.814	2.787	2.830	2.788	2.725	2.690	2.783	2.762	2.642	2.638

Table 5 Pauling bond orders and tightness parameters for reactant complexes and transition structures for Cl⁻ + R-Cl

Method	R	$n(\text{C}\cdots\text{Cl}_{\text{nuc}})^{\text{RC}}$	$n(\text{C}\cdots\text{Cl}_{\text{lg}})^{\text{RC}}$	τ^{RC}	$n(\text{C}\cdots\text{Cl}_{\text{nuc}})^{\text{TS}}$	$n(\text{C}\cdots\text{Cl}_{\text{lg}})^{\text{TS}}$	τ^{TS}	$\Delta\tau^\ddagger$
HF ($c = 0.86$)	Me	0.18	0.95	1.13	0.50	0.50	1.00	-0.13
	Et	0.15	0.95	1.10	0.45	0.46	0.91	-0.19
	Pr ⁱ	0.11	0.95	1.06	0.41	0.41	0.81	-0.25
	Bu ^t	0.05	0.96	1.01	0.26	0.26	0.53	-0.49
B3LYP ($c = 0.81$)	Me	0.21	0.93	1.13	0.50	0.50	1.00	-0.13
	Et	0.15	0.96	1.11	0.46	0.50	0.96	-0.15
	Pr ⁱ	0.12	0.96	1.10	0.44	0.44	0.89	-0.19
	Bu ^t	0.11	0.96	1.07	0.34	0.34	0.67	-0.39
MP2 ($c = 0.75$)	Me	0.16	0.97	1.13	0.50	0.50	1.00	-0.13
	Et	0.13	0.97	1.10	0.48	0.48	0.97	-0.13
	Pr ⁱ	0.08	0.98	1.06	0.45	0.45	0.89	-0.16
	Bu ^t	0.07	0.98	1.05	0.35	0.35	0.69	-0.36
PCM/HF ($c = 0.86$)	Me	0.17	0.98	1.15	0.50	0.50	1.00	-0.15
	Et	0.14	0.98	1.13	0.43	0.45	0.88	-0.24
	Pr ⁱ	0.14	0.99	1.13	0.37	0.38	0.75	-0.38
	Bu ^t	0.12	0.98	1.10	0.23	0.23	0.45	-0.64
PCM/B3LYP ($c = 0.79$)	Me	0.18	0.97	1.15	0.50	0.50	1.00	-0.15
	Et	0.15	0.97	1.12	0.45	0.47	0.92	-0.20
	Pr ⁱ	0.09	0.97	1.06	0.40	0.41	0.82	-0.25
	Bu ^t	0.06	0.98	1.04	0.27	0.27	0.54	-0.50

Cossi *et al.*²¹ have studied the Cl⁻ + MeCl reaction in water by means of a conductor PCM + density functional method, but we are unaware of theoretical studies including solvation for R = Et, Prⁱ, Bu^t. Our PCM/6-31G* results indicate higher barriers for the reactions in water as compared with *in vacuo*; as expected, the solvent stabilises the localized charge on the isolated chloride anion, or on the Cl⁻ moiety within the RC, more than the delocalized charge in the TS. Increasing α -alkylation raises the barrier height in the PCM/B3LYP and PCM/MP2 calculations, similarly to the vacuum results, but the PCM/HF results for R = Prⁱ and Bu^t surprisingly show the opposite trend. Nonetheless, the general trend is clear: increasing α -alkylation tends to

raise the barrier height for the Cl⁻ + RCl identity S_N2 reactions.

The lower part of Fig. 1 shows barrier heights calculated for H₂O + R-OH₂⁺ identity reactions in a vacuum and in water. Our vacuum results essentially agree with those for backside S_N2 reaction reported by Uggerud and Bache-Andreassen⁵ using the same methods, although the energy barriers we present here are relative potential energies without zero-point energy corrections. Not surprisingly we therefore obtain the same trend for the effect of increasing α -alkylation upon the barrier height. B3LYP/6-31G* and MP2/6-31G* both show a small increase in barrier from R = Me to R = Et, followed by decreases for R = Prⁱ and R = Bu^t, whereas HF/6-31G* shows a

Table 6 Pauling bond orders and tightness parameters for reactant complexes and transition structures for $\text{H}_2\text{O} + \text{R-OH}_2^+$

Method	R	$n(\text{C}\cdots\text{O}_{\text{nuc}})^{\text{RC}}$	$n(\text{C}\cdots\text{O}_{\text{lg}})^{\text{RC}}$	τ^{RC}	$n(\text{C}\cdots\text{O}_{\text{nuc}})^{\text{TS}}$	$n(\text{C}\cdots\text{O}_{\text{lg}})^{\text{TS}}$	τ^{TS}	$\Delta\tau^\ddagger$
HF ($c = 0.76$)	Me	0.21	0.97	1.18	0.50	0.50	1.00	-0.18
	Et	0.17	0.97	1.14	0.42	0.42	0.84	-0.30
	Pr ⁱ	0.15	0.97	1.12	0.26	0.35	0.61	-0.51
	Bu ^t	0.09	0.90	0.99	0.22	0.23	0.45	-0.54
B3LYP ($c = 0.65$)	Me	0.19	0.95	1.14	0.50	0.50	1.00	-0.14
	Et	0.14	0.97	1.11	0.44	0.44	0.89	-0.22
	Pr ⁱ	0.13	0.97	1.10	0.37	0.37	0.75	-0.36
	Bu ^t	0.07	0.88	0.95	0.16	0.17	0.33	-0.62
MP2 ($c = 0.64$)	Me	0.18	0.95	1.13	0.50	0.50	1.00	-0.13
	Et	0.08	0.97	1.05	0.45	0.45	0.90	-0.15
	Pr ⁱ	0.06	0.98	1.04	0.35	0.35	0.70	-0.34
	Bu ^t	0.06	0.96	1.02	0.17	0.18	0.36	-0.66
PCM/HF ($c = 0.71$)	Me	0.19	0.96	1.15	0.50	0.50	1.00	-0.15
	Et	0.15	0.96	1.12	0.44	0.44	0.87	-0.25
	Pr ⁱ	0.13	0.96	1.10	0.36	0.36	0.72	-0.37
	Bu ^t	0.08	0.89	0.97	0.21	0.21	0.42	-0.55
PCM/B3LYP ($c = 0.63$)	Me	0.18	0.95	1.13	0.50	0.50	1.00	-0.13
	Et	0.14	0.97	1.10	0.47	0.47	0.94	-0.16
	Pr ⁱ	0.12	0.99	1.11	0.42	0.42	0.84	-0.27
	Bu ^t	0.06	0.88	0.94	0.21	0.21	0.41	-0.53

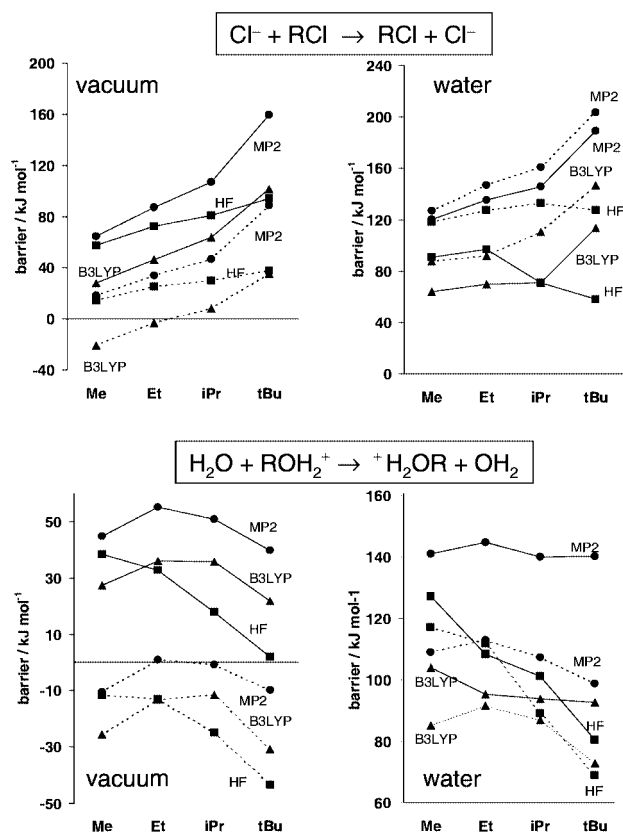


Fig. 1 Effect of α -alkylation upon potential energy barriers (kJ mol^{-1}) for $\text{S}_{\text{N}}2$ identify reactions $\text{Cl}^- + \text{RCl}$ (upper panels) and $\text{H}_2\text{O} + \text{R-OH}_2^+$ (lower panels) *in vacuo* (left-hand panels) and in water (right-hand panels) with $\text{R} = \text{Me, Et, Pr}^i$ and Bu^t . Solid lines denote energies $\Delta E_{\text{rc}}^\ddagger$ of transition structures relative to reactant complexes; dotted lines denote energies $\Delta E_{\text{r}}^\ddagger$ relative to separated reactants. Squares (■) denote HF/6-31G*, triangles (▲) denote B3LYP/6-31G*, and circles (●) denote MP2/6-31G*; aqueous solvation is described by the polarizable continuum model.

monotonic decrease in barrier height along the series from Me to Bu^t . The energy barriers $\Delta E_{\text{r}}^\ddagger$ (dotted lines in Fig. 1) are all lower than the values of $\Delta E_{\text{rc}}^\ddagger$ (solid lines) by the amount of ΔE_{assoc} .

Our PCM/MP2/6-31G* calculated values for $\Delta E_{\text{rc}}^\ddagger$ are remarkably insensitive to the degree of α -alkylation in $\text{H}_2\text{O} + \text{R-OH}_2^+$, whereas $\Delta E_{\text{r}}^\ddagger$ behaves similarly to the HF barriers for $\text{Cl}^- + \text{RCl}$, with values in the order $\text{Me} < \text{Et} > \text{Pr}^i > \text{Bu}^t$. We were unable to re-optimize the geometries with PCM/MP2 since Gaussian 98 does not provide gradients for this method; therefore these PCM/MP2 barriers were obtained from single-point PCM/MP2/6-31G*//MP2/6-31G* energies. The PCM/B3LYP and PCM/HF values for $\Delta E_{\text{rc}}^\ddagger$ decrease monotonically along the series $\text{Me} > \text{Et} > \text{Pr}^i > \text{Bu}^t$, as do the PCM/HF values for $\Delta E_{\text{r}}^\ddagger$. Uggerud and Bache-Andreassen⁵ performed calculations containing an additional four water molecules to solvate the RCs and TSs, and found that the energy barriers for these clusters were in the order $\text{Me} < \text{Et} < \text{Pr}^i < \text{Bu}^t$, in accord with the conventional expectation for $\text{S}_{\text{N}}2$ reactions in solution. However, in hybrid QM/MM studies involving explicit solvation of these reactions by several hundred water molecules,²² we have found that the first solvation shell of $\text{H}_2\text{O} + \text{R-OH}_2^+$ contains somewhere between 20 and 35 water molecules as R is changed from Me to Bu^t . It is therefore dubious whether a cluster containing only four additional water molecules can provide a realistic model for aqueous solution. We therefore consider that the present PCM results may be more indicative of the effect of aqueous solvation upon these reactions than are gas-phase supermolecule calculations on small micro-solvated clusters. The trend in our PCM results is clear: increasing α -alkylation does *not* raise the barrier to backside $\text{S}_{\text{N}}2$ reaction of water with protonated alcohols; if anything, increasing α -alkylation tends to reduce the barrier height.

The addition of methyl groups on the α -carbon increases both the $\text{C}\cdots\text{O}_{\text{nuc}}$ and $\text{C}\cdots\text{O}_{\text{lg}}$ distances in all the structures *in vacuo*. In particular, the TSs become progressively looser and, with τ^{TS} in the range 0.33 to 0.45, that for $\text{R} = \text{Bu}^t$ is certainly an example of an exploded²³ $\text{S}_{\text{N}}2$ TS. Moreover, the values of τ^{TS} are much smaller, and those of $\Delta\tau^\ddagger$ much larger, for $\text{H}_2\text{O} + \text{R-OH}_2^+$ than for $\text{Cl}^- + \text{RCl}$; the R group in the TSs for the former reactions becomes increasingly carbocationic in character as the degree of α -methylation increases. Solvation by the PCM method has very little effect upon the RCs, but serves to tighten the $\text{C}\cdots\text{O}$ bonds in the TS as compared to their *vacuo* values. The Pauling bond orders, tightness parameters

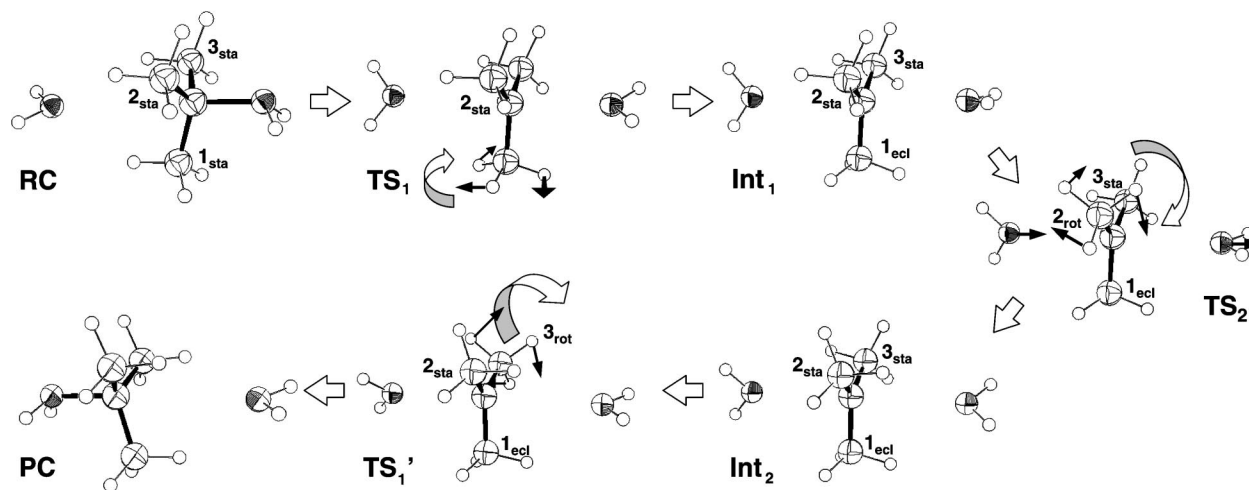


Fig. 2 Stationary structures along the reaction coordinate for $\text{H}_2\text{O} + \text{Bu}'\text{-OH}_2^+$ identify $\text{S}_{\text{N}}2$ showing the timing of methyl group rotations.

and $\Delta\tau^\ddagger$ values for $\text{H}_2\text{O} + \text{R-OH}_2^+$ and $\text{Cl}^- + \text{RCl}$ in water are remarkably similar.

The decrease in $\text{S}_{\text{N}}2$ reactivity (increase in barrier height) from $\text{R} = \text{Me}$ to $\text{R} = \text{Bu}'$ for reactions of anionic nucleophiles with neutral electrophiles is usually understood as being due to steric repulsion in the transition state between the nucleophile and the α -methyl substituent groups. The magnitude of the steric component of the TS for $\text{R} = \text{Bu}'$ *in vacuo* may be estimated by means of the following procedure. The α -carbon atom of the TS may be deleted and replaced by a capping hydrogen atom located along each of the $\text{C}_\alpha\text{-CH}_3$ bonds, whilst maintaining a frozen geometry; the energy of this supermolecule may be calculated. The nucleophile and leaving group may then be deleted, and the energy of the "methane trimer" fragment determined. Finally, the methane trimer may be deleted, and the energy of the nucleophile and leaving group fragment evaluated, still with frozen geometry. The energy difference between the supermolecule and the sum of the fragments provides a measure of the steric interaction. At the HF/6-31G* level this procedure yields a steric energy of 733 kJ mol^{-1} for the $\text{Cl}^- + \text{Bu}'\text{-Cl}$ TS. However, the same procedure applied to the $\text{H}_2\text{O} + \text{Bu}'\text{-OH}_2^+$ TS gives a steric energy of only -1 kJ mol^{-1} ! This result lends support to the suggestion of Uggerud and Bache-Andreassen⁵ that our ideas of steric hindrance should be revised to take account of the nature of the nucleophile as well as of the α -alkyl substituents.

How does the combination of an anionic nucleophile + neutral electrophile differ from that of a neutral nucleophile + cationic electrophile? The answer is not that they have a different number of valence electrons, but rather that they have a different number of protons. This is clear if one considers $\text{HO}^- + \text{R-OH}$ vs. $\text{H}_2\text{O} + \text{R-OH}_2^+$. If one proton is deleted from the nucleophile and one from the leaving group for the RCs and TSs, with frozen geometries, the HF/6-31G* calculated potential energy barriers *in vacuo* are 126 and 244 kJ mol^{-1} for $\text{R} = \text{Me}$ and Bu' , respectively. After relaxation of the RC and TS geometries for $\text{HO}^- + \text{R-OH}$ to fully refined stationary points, these values change very little, to 120 and 218 kJ mol^{-1} , respectively. These barriers may be compared with the values of 38 and 2 for $\text{H}_2\text{O} + \text{R-OH}_2^+$ with $\text{R} = \text{Me}$ and Bu' , respectively. It would appear that the presence of two additional protons in the neutral nucleophile + cationic electrophile system not only greatly reduces the steric repulsion of the α -methyl substituents, but also reduces the interaction with C_α itself.

Timing of methyl group rotations occurring during nucleophilic substitution

Transition vectors calculated with all methods for $\text{S}_{\text{N}}2$

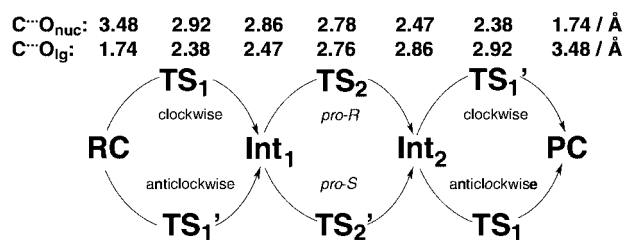


Fig. 3 Alternative reaction paths for $\text{H}_2\text{O} + \text{Bu}'\text{-OH}_2^+$ methyl group rotations; bond lengths are for PCM/HF/6-31G*.

reactions with $\text{R} = \text{Me}$ reveal classic Walden inversion. The α -methyl group in a RC with $\text{R} = \text{Et}$ is staggered with respect to the CH_2X group, with one hydrogen atom being antiperiplanar to the leaving group X. If an $\text{S}_{\text{N}}2$ identity reaction involves *only* Walden inversion at C_α , the product complex (PC) must have its CH_3 group eclipsed relative to CH_2X , with one H being synperiplanar to X. In order to obtain a PC equivalent to the RC, it is necessary for internal rotation about the $\text{C}_\alpha\text{-C}_\beta$ bond to occur, in addition to the antisymmetric stretching of the bonds to the nucleophile and the leaving group. Streitwieser *et al.*²⁴ have noted for $\text{Cl}^- + \text{Et-Cl}$ that these are two distinct normal modes in the TS, and our calculations concur that the $\text{C}_\alpha\text{-C}_\beta$ torsion contributes only a little to the transition vector. Our calculations for $\text{H}_2\text{O} + \text{Et-OH}_2^+$ suggest that these motions are strongly coupled in the transition vector. The same coupling must also occur in the TS for concerted $\text{S}_{\text{N}}2$ identity reactions with $\text{R} = \text{Pr}^i$, although its contribution to the transition vector is disguised as a tilting motion of the whole Pr^i group. Rotation of the two CH_3 groups occurs in opposite senses and allows a plane of symmetry to be conserved along the whole length of the reaction coordinate from RC to PC *via* a TS with C_{2v} symmetry. The HF/6-31G* method for $\text{H}_2\text{O} + \text{Pr}^i\text{-OH}_2^+$ *in vacuo* behaves a little differently: it shows the C_{2v} species as an intermediate lying in a shallow well about 0.1 kJ mol^{-1} below the equivalent pair of slightly asymmetric TSs found just before and after it along the reaction coordinate.

The situation for $\text{R} = \text{Bu}'$ is more complicated than has generally been recognized. Let us first describe the reaction coordinate for $\text{H}_2\text{O} + \text{Bu}'\text{-OH}_2^+$. In principle the rotations of the three CH_3 groups could occur simultaneously and in concert with the antisymmetric stretch of the $\text{C}\cdots\text{O}_{\text{nuc}}$ and $\text{C}\cdots\text{O}_{\text{lg}}$ bonds. In practice, all theoretical methods employed in this study predict that the three CH_3 groups' rotations occur sequentially in a stepwise manner, as illustrated by Figs. 2 and 3. The leaving group water in RC is pyramidal while the nucleophilic water is planar, and $\text{C}\cdots\text{O}_{\text{nuc}} \gg \text{C}\cdots\text{O}_{\text{lg}}$. As the nucleophile approaches and the leaving group departs, both water moieties become planar, with their local symmetry axes

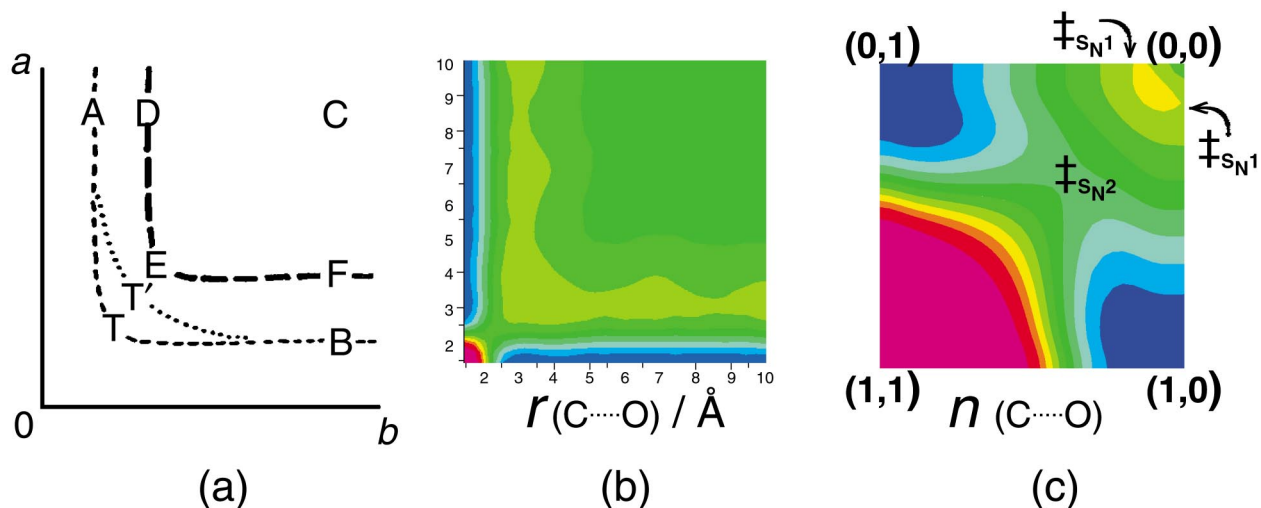


Fig. 4 (a) Sketch of imaginary PES from Hughes, Ingold and Shapiro (ref. 25), and AM1/COSMO calculated energy surface for $\text{H}_2\text{O} + \text{Et-OH}_2^+$ in (b) bond distance coordinates and (c) bond order coordinates (red = high energy, blue = low energy).

aligned with the $\text{O}_{\text{nuc}} \cdots \text{C} \cdots \text{O}_{\text{lg}}$ axis, and remain so until **PC** is reached. Also in **RC** each CH_3 group ($\mathbf{1}_{\text{sta}}$, $\mathbf{2}_{\text{sta}}$ and $\mathbf{3}_{\text{sta}}$) is staggered with respect to the $\text{C} \cdots \text{O}_{\text{lg}}$ bond. In the first step, one of the CH_3 groups rotates into the orientation ($\mathbf{1}_{\text{ecl}}$) found ultimately in **PC**, in which it is staggered with respect to $\text{C} \cdots \text{O}_{\text{nuc}}$ but eclipsed relative to $\text{C} \cdots \text{O}_{\text{lg}}$. In **TS**₁ this rotation ($\mathbf{1}_{\text{rot}}$) is coupled to the antisymmetric $\text{C} \cdots \text{O}_{\text{nuc}}/\text{C} \cdots \text{O}_{\text{lg}}$ stretch, and $\text{C} \cdots \text{O}_{\text{nuc}}$ is still considerably longer than $\text{C} \cdots \text{O}_{\text{lg}}$. The energy of **TS**₁ is only slightly lower (or slightly higher in the case of PCM/HF/6-31G*) than that of **TS**₂. The first intermediate **Int**₁ lies no more than 1.5 kJ mol^{-1} below **TS**₁. In the second step another CH_3 group undergoes rotation ($\mathbf{2}_{\text{rot}}$) via **TS**₂ to a second intermediate **Int**₂ that is entirely equivalent to **Int**₁. Both have an essentially planar Bu' moiety with one CH_3 group having a C-H bond pointing towards one H_2O moiety, and the other two CH_3 groups having C-H bonds pointing towards the other H_2O . The third step involves rotation of the last CH_3 group ($\mathbf{3}_{\text{rot}}$) via **TS**₃, which is actually the enantiomer of **TS**₁. Uggerud and Bache-Andreassen⁵ have described the same behaviour for this reaction *in vacuo* as we now report for the reaction in PCM water also.

Closer analysis reveals a further degree of subtlety. The first CH_3 group rotation may occur in either a clockwise or an anticlockwise sense. Fig. 2 shows a clockwise rotation, as viewed from C_a , leading to **TS**₁, which is a chiral species. Anticlockwise rotation would lead directly to its enantiomer **TS**_{1'} (\equiv **TS**₃) along a mirror-image reaction path (Fig. 3). Any one of the three equivalent CH_3 groups may be involved in the first step. The second step, from **Int**₁ to **Int**₂, may also involve either of the two equivalent CH_3 groups. Clockwise or anticlockwise rotation of CH_3 group **2** leads to one and the same species **TS**₂. However, either clockwise or anticlockwise rotation of CH_3 group **3** leads to **TS**_{2'}, the enantiomer of **TS**₂. The third step is the reverse of the first: clockwise rotation of the last CH_3 group leads to **TS**₃ (\equiv **TS**_{1'}), whereas anticlockwise rotation leads to its enantiomer **TS**₁. The intermediate **Int**₁ \equiv **Int**₂ is achiral, but the reaction paths interconnecting them are enantiomeric. If one accepts the eclipsed methyl group $\mathbf{1}_{\text{ecl}}$ as being different from the staggered ones $\mathbf{2}_{\text{sta}}$ and $\mathbf{3}_{\text{sta}}$, and, furthermore, assigns it a higher priority in the Cahn-Ingold-Prelog sense, then the two paths from **Int**₁ may be distinguished. The CH_3 group labeled $\mathbf{2}_{\text{sta}}$ could be considered as being *pro-R* (with respect to the leaving group, $\mathbf{1}_{\text{ecl}}$ and $\mathbf{3}_{\text{sta}}$), whereas that labeled $\mathbf{3}_{\text{sta}}$ could be considered as *pro-S* (Fig. 3).

A consequence of the chirality of **TS**₂ is that there is no requirement for the bond lengths to the nucleophile and leaving group to be equal, even though this species is the pivotal point along the overall reaction pathway for the identity reaction.

Nonetheless, these bond distances are not very different, and it is of interest to enquire what structure results from a constrained optimization in which $\text{C} \cdots \text{O}_{\text{nuc}}$ and $\text{C} \cdots \text{O}_{\text{lg}}$ are set equal. The answer is a species with $\text{C} \cdots \text{O}_{\text{nuc}} = \text{C} \cdots \text{O}_{\text{lg}} = 2.716 \text{ \AA}$, that satisfies the usual convergence criteria for geometry optimization to an energy minimum. Its vibrational frequencies are all real, but the root-mean-square (RMS) residual force is $11 \times 10^{-5} E_{\text{h}}/a_0$ compared with only $8 \times 10^{-6} E_{\text{h}}/a_0$ for the asymmetric structure **Int**, which is 2.4 kJ mol^{-1} lower in energy. Furthermore, we have characterized the $\text{C}_{3\text{h}}$ symmetrical species in which not only are $\text{C} \cdots \text{O}_{\text{nuc}}$ and $\text{C} \cdots \text{O}_{\text{lg}}$ set equal, but also all three CH_3 groups are rotated in the same direction with one C-H bond lying in the symmetry plane. This species is a third-order saddle point ($160i, 137i, 109i \text{ cm}^{-1}$) with $\text{C} \cdots \text{O}_{\text{nuc}} = \text{C} \cdots \text{O}_{\text{lg}} = 2.709 \text{ \AA}$, lying 4 kJ mol^{-1} above **TS**₂.

The reaction coordinate for $\text{Cl}^- + \text{Bu}'\text{-Cl}$ is simpler but still intriguing. The same three CH_3 group rotations occur in distinct stages of a concerted process involving a single TS. The first rotation occurs completely during the “uphill” stage, and the third rotation occurs completely during the “downhill” stage. The transition vector shows rotation of only the second CH_3 group coupled with the antisymmetric $\text{C} \cdots \text{Cl}_{\text{nuc}}/\text{C} \cdots \text{Cl}_{\text{lg}}$ stretching motion. The structure reported by Jensen¹⁶ as the TS is not a true stationary point; it resembles the intermediate **Int** for $\text{H}_2\text{O} + \text{Bu}'\text{-OH}_2^+$. Since the potential energy surface is quite flat in the saddle region, great care must be taken with geometry optimization to converge towards stationary points with zero gradients. The species obtained from constrained optimization with equal $\text{C} \cdots \text{Cl}_{\text{nuc}}$ and $\text{C} \cdots \text{Cl}_{\text{lg}}$ bond distances is apparently a first-order saddle point (429i) with $\text{C} \cdots \text{Cl}_{\text{nuc}} = \text{C} \cdots \text{Cl}_{\text{lg}} = 2.629 \text{ \AA}$. It is 0.15 kJ mol^{-1} higher in energy than the true TS, but although its RMS residual force is, at $15 \times 10^{-6} E_{\text{h}}/a_0$, well below the usual threshold for convergence, it is still greater than the value of $5 \times 10^{-6} E_{\text{h}}/a_0$ achieved for the asymmetric TS.

S_N2/S_N1 mechanistic changeover in nucleophilic aliphatic substitution

Hughes, Ingold and Shapiro²⁵ have described the mechanistic changeover from $\text{S}_{\text{N}}2$ to $\text{S}_{\text{N}}1$ observed for aliphatic nucleophilic substitution [eqn. (1), $\text{X} = \text{HO}$, $\text{Y} = \text{Br}$] of simple bromoalkanes by hydroxide anion in 60% aqueous ethanol with increasing methylation on the α -carbon atom. Reactions with $\text{R} = \text{Me}$ or Et were bimolecular, whereas those with $\text{R} = \text{Pr}^i$ or Bu' were unimolecular. Their discussion invited the reader to consider how the changing topography of an imaginary potential energy

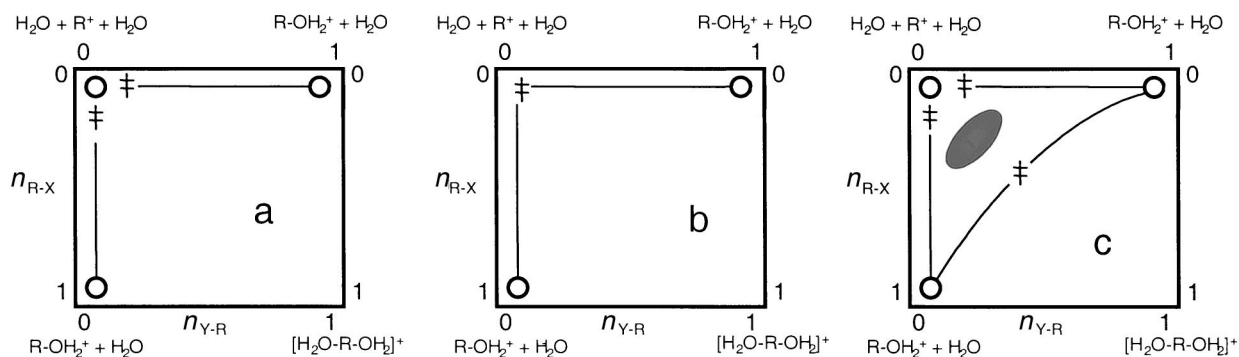


Fig. 5 More O'Ferrall-Jencks diagrams depicting mechanistic change. The changeover from S_N2 (a) to S_N1 reaction mechanism could occur by an S_N2 (b) reaction with essentially the same structure as the S_N1 intermediate or an S_N1 and S_N2 (c) pathway running concurrently.

surface (PES, Fig. 4a) governing these reactions would lead not only to a shift in the location of the transition state but also to a switch from a concerted to a stepwise mechanism. Thus α -alkylation would cause the saddle-point T along the reaction path from reactants A to products B to shift to T' and, in due course, to breach the ridge DEF separating the concerted mechanism from the plateau corresponding to the intermediate C of the stepwise mechanism.

It is now straightforward to perform molecular orbital calculations for such a family of reactions and to construct the PESs previously only imagined by Ingold and co-workers in 1936. For simplicity we have performed AM1/COSMO calculations for $H_2O + R-OH_2^+$. Fig. 4b shows a contour map of the calculated enthalpy surface, for $R = Et$, as a function of the bond lengths for the making and breaking $C \cdots O$ bonds involving the nucleophile and leaving group. There is a very satisfying resemblance between this calculated surface and Ingold's sketch map (Fig. 4a). The contour map (not shown) for reaction of $Cl^- + Et-Cl$ in water is qualitatively very similar.

Fig. 4c depicts the AM1/COSMO calculated enthalpy surface transformed into bond order coordinates $n(C \cdots O)$ for $H_2O + Et-OH_2^+$. (A value of $c = 0.67$ for the coefficient in the Pauling bond order expression is obtained by the procedure described above.) The striking result is that the topographical feature of most chemical interest, the saddle region corresponding to the S_N2 TS, \ddagger_{S_N2} , now dominates the contour plot, whereas in Fig. 4b it is confined to a small corner of the map. Moreover, the form of the surface expressed in bond order coordinates is approximately quadratic.²⁶ The plateau region C of Figs. 4a and 4b, however, now appears as a local energy minimum in the (0,0) corner of Fig. 4c. Clearly it may be seen that there is a concerted reaction path leading diagonally from reactants to products by means of the TS \ddagger_{S_N2} . However, there is also a stepwise reaction path that runs horizontally along the edge from (0,1) to (0,0) via TS \ddagger_{S_N1} and then vertically along the edge from (0,0) to (1,0) through an equivalent S_N1 TS.

Jencks²⁷ has discussed possible ways by which an S_N1 mechanism could change to an S_N2 mechanism, which may be illustrated by the More O'Ferrall-Jencks (MOFJ) diagrams shown in Fig. 5. The S_N1 mechanism (Fig. 5a) involves an intermediate in the top-left corner corresponding to an energy well on the PES, represented by an open circle; there is one TS for its formation and a second for its breakdown. Destabilization would cause the depth of this energy well and lifetime of the intermediate to diminish. As this lifetime becomes comparable with the period of a molecular vibration, the three critical points (two saddle points and one minimum) on the stepwise reaction path coalesce to a single saddle point. This corresponds to a TS for a concerted reaction having a structure and energy essentially the same as that of the now disappeared S_N1 intermediate. This possibility (Fig. 5b) was discussed originally by Doering and Zeiss.²⁸ Alternatively, the S_N1 intermediate may co-exist with the S_N2 TS, being separated from it by an energy maximum, represented by the shaded region

on Fig. 5c. The S_N1 and S_N2 pathways occur in parallel and traverse different regions of the MOFJ diagram, despite being of equal energy at the point of mechanistic change.

Barnes, Wilkie and Williams (BWW)²⁹ performed AM1 calculations for $H_2O + R-OH_2^+$ *in vacuo*. In particular, PESs were determined for $R = Et$ and $MeOCH_2$ in the same way as above. The two surfaces were similar in their overall form, but the energy contours revealed a striking dissimilarity in the region of the S_N2 TS and S_N1 intermediate: the one for $R = MeOCH_2$ contained a shallow well (0.6 kJ mol^{-1}) at the same location as the TS for $R = Et$. It appeared that the changeover in mechanism occurred in a structurally continuous way as described by the Doering and Zeiss model. However, the BWW study did not include any treatment of solvation.

Fig. 6 contains AM1/COSMO enthalpy surfaces to illustrate the changing topography accompanying S_N2/S_N1 mechanistic changeover along the series $R = Me, Et, Pr^i$ and Bu^i for $H_2O + R-OH_2^+$. As C_α becomes increasingly methylated, the (0,0) corner of the surface, corresponding to the carbocation R^+ with two molecules of water at infinite separation, is lowered in energy owing to the stabilizing inductive effects of the methyl groups. Conversely, the energy of the (1,1) corner, corresponding to the pentacoordinate adduct of an associative mechanism, is raised. Thus the surfaces become increasingly tilted in the direction of the tricoordinate intermediate of the dissociative mechanism, and the S_N2 TS slides towards this (0,0) corner. The color range from blue (low energy) to red (high energy) on each of these surfaces has been adjusted in order to emphasize the subtle changes in the topography of the TSs \ddagger_{S_N2} and \ddagger_{S_N1} . It is evident that the concerted S_N2 mechanism is preferred for $R = Me$ and Et , since for these alkyl groups the energy of \ddagger_{S_N2} is less than that of \ddagger_{S_N1} . The changeover to the stepwise S_N1 mechanism favored for $R = Pr^i$ and Bu^i occurs by a see-saw process which results in \ddagger_{S_N1} becoming lower in energy than \ddagger_{S_N2} . A hypothetical degree of alkylation at C_α would involve the energies of \ddagger_{S_N2} and \ddagger_{S_N1} being equal and (neglecting entropic contributions) nucleophilic substitution taking place by both mechanisms equally. To either side of this "point of balance" the reaction follows each pathway according to the Boltzmann populations of the competing TSs as determined by their relative energies.

Table 7 contains AM1/COSMO enthalpies of activation for these reactions in water. The values of ΔH^\ddagger are similar to the PCM/HF/6-31G* values for ΔE_r^\ddagger (Table 2) and show the same decreasing trend with increasing α -methylation. Moreover, the TS bond orders are also very similar. This agreement with *ab initio* results lends support to our use of a semiempirical MO method for mapping out the entire surfaces for this series of reactions. Comparison of AM1/COSMO enthalpies of hydration $\Delta_h H(R^+)$ for the carbocations with Abraham's (estimated) values³⁰ suggests that our calculated results may be overestimated, particularly for the smaller ions. We have simply used the default parameters in the MOPAC93 implementation of the COSMO method, but it may be that better

Table 7 AM1/COSMO calculated energy barriers (kJ mol^{-1}), TS bond lengths (\AA), Pauling bond orders and 2° α -deuterium kinetic isotope effects (298 K, per D) for $\text{H}_2\text{O} + \text{R-OH}_2^+$

	$\text{S}_{\text{N}}2$				$\text{S}_{\text{N}}1$				$\Delta_{\text{h}}H(\text{R}^+)$	
	ΔH^\ddagger	$\text{C}\cdots\text{O}$	$n(\text{C}\cdots\text{O})^{\text{TS}}$	$k_{\text{H}}/k_{\text{D}}$	ΔH^\ddagger	$\text{C}\cdots\text{O}$	$n(\text{C}\cdots\text{O})^{\text{TS}}$	$k_{\text{H}}/k_{\text{D}}$	Calc.	Lit. ^a
Me	91.7	1.94	0.50	1.01	136.1	3.30	0.07	1.36	-400	-322
Et	84.3	2.08	0.41	1.10	104.6	2.90	0.12	1.28	-330	-274
Pr ⁱ	57.6	2.30	0.29	1.17	51.1	2.73	0.15	1.25	-285	-253
Bu ^t	31.5	2.49	0.22		18.1	2.36	0.27		-256	-236
MeOCH ₂	51.2	2.11	0.39	1.16	54.2	3.01	0.10	1.29		
MeOCHMe	31.2	2.24	0.32	1.15	24.3	2.18	0.35	1.20		

^a See ref. 30.

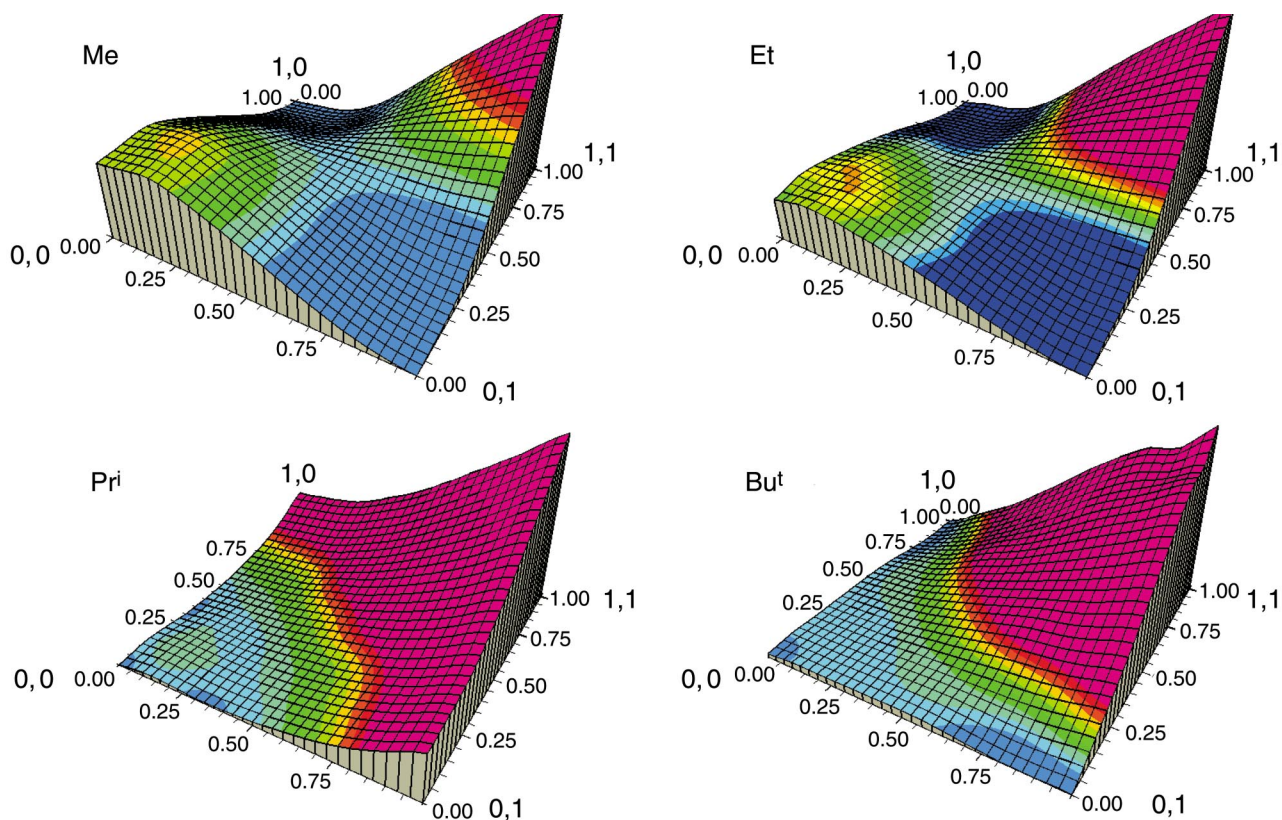


Fig. 6 AM1/COSMO calculated energy surfaces for $\text{H}_2\text{O} + \text{R-OH}_2^+$ ($\text{R} = \text{Me}, \text{Et}, \text{Pr}^i$ and Bu^t) in bond order coordinates.

agreement could be obtained by alteration of the van der Waals' radius for the C_α^+ used to define the solvent-accessible surface around each carbocation.

The effect of the COSMO solvation method upon the AM1 enthalpy surfaces calculated for $\text{R} = \text{MeOCH}_2$ and $\text{R} = \text{MeOCHMe}$ is shown in Fig. 7. A methoxy substituent on C_α lowers the energy of the (0,0) corner on the vacuum surface relative to a methyl substituent alone, but this corner is an energy maximum, and the $\text{S}_{\text{N}}2$ path is the only route across the surface. The surface published by BWW²⁵ for $\text{R} = \text{MeOCH}_2$ was plotted in bond distance coordinates and corresponded to only a small region of the surface shown here in bond order coordinates. The surface for reaction in water shows both $\text{S}_{\text{N}}1$ and $\text{S}_{\text{N}}2$ paths, as for the simple alkyl substrates. There is no shallow minimum on this surface at the location of the saddle point on the $\text{R} = \text{Et}$ surface. The COSMO solvation energy is largest (most negative; blue color) for those species in which the charge is most localized: that is, the reactants, products and the isolated cation at the (0,0) corner. It is smallest (least negative; red color) for the symmetrically solvated cation ($\text{H}_2\text{O}\cdots\text{R}\cdots\text{OH}_2^+$). The effect of solvation by the continuum is to turn the (0,0) corner from a maximum to a minimum. The additional α -methyl substituent present in $\text{R} = \text{MeOCHMe}$ stabilizes the ($\text{H}_2\text{O}\cdots\text{R}\cdots\text{OH}_2^+$) cation to such an extent that

this species is the global minimum on this surface *in vacuo*. The rounded peak in the solvation energy surface "fills" the ($\text{H}_2\text{O}\cdots\text{R}\cdots\text{OH}_2^+$) basin in the vacuum surface, leading to a rather flat plateau in this region of the surface in water, although both $\text{S}_{\text{N}}1$ and $\text{S}_{\text{N}}2$ paths now exist.

Kinetic isotope effects

AM1/COSMO calculated secondary kinetic isotope effects (KIEs) $k_{\text{H}}/k_{\text{D}}$ for substitution of a single deuterium on C_α are given in Table 7 for both $\text{S}_{\text{N}}2$ and $\text{S}_{\text{N}}1$ mechanisms for the reactions $\text{H}_2\text{O} + \text{R-OH}_2^+$. The isotope effect for $\text{S}_{\text{N}}2$ reaction with $\text{R} = \text{Me}$ is very weak (close to unity), but its value becomes stronger (>1) as increasing substitution by methyl or methoxy on C_α leads to increasing stability of the carbocation moiety R^+ in the $\text{S}_{\text{N}}2$ TS, and to smaller TS bond orders, as previously reported for $\text{Cl}^- + \text{R-Cl}$.³¹ Inspection of the calculated results for the $\text{S}_{\text{N}}1$ mechanism shows the opposite behavior. As the stability of the carbocation increases, so the $\text{S}_{\text{N}}1$ TS is tighter (larger $\text{C}\cdots\text{O}$ bond order) and the 2° α -D KIE is weaker (less normal). Although 2° α -D KIEs have not been determined experimentally for these identity reactions, the calculated values 1.01 for $\text{R} = \text{Me}$ and 1.10 for $\text{R} = \text{Et}$ are both reasonable for $\text{S}_{\text{N}}2$ mechanisms, but the value of 1.17 for $\text{R} = \text{Pr}^i$ is in the range

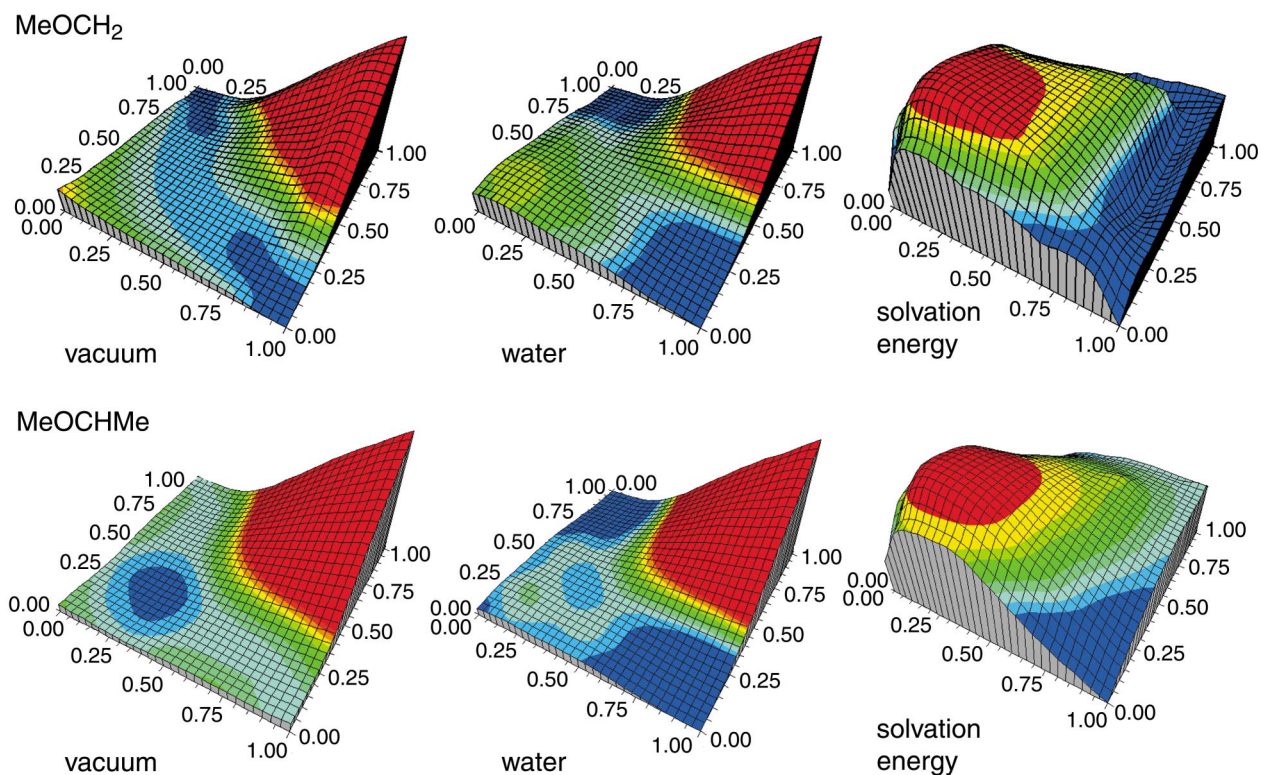


Fig. 7 AM1 calculated energy surfaces for $\text{H}_2\text{O} + \text{R}-\text{OH}_2^+$ ($\text{R} = \text{MeOCH}_2$ and MeOCHMe) in bond order coordinates in both a vacuum and water (COSMO), and the solvation energy computed as the difference between the previous two surfaces.

usually attributed to an $\text{S}_{\text{N}}1$ mechanism. However, the calculated value of 1.25 for $\text{R} = \text{Pr}^i$ actually going by the $\text{S}_{\text{N}}1$ mechanism is also entirely plausible. Table 7 also contains KIEs for mechanisms that would not be observable experimentally. For example, we predict α -D KIEs of 1.36 and 1.28 for $\text{S}_{\text{N}}1$ reactions of the primary substrates with $\text{R} = \text{Me}$ and Et , respectively. All the trends in these calculated results are consistent with qualitative predictions that may be made on the basis of a simple MOFJ diagram.²⁹

Conclusion

Does the relative rate of bimolecular nucleophilic substitution between a neutral nucleophile Nu and a cationic electrophile $\text{R}-\text{Z}^+$ decrease along the series $\text{R} = \text{Me}$, Et , Pr^i and Bu^t ? According to our calculated potential energy barrier heights *in vacuo* and in water for identity reactions $\text{H}_2\text{O} + \text{R}-\text{OH}_2^+$, the answer is no. The additional proton on both the nucleophile and leaving group dramatically reduces the repulsion interaction between these groups and α -methyl substituents, as compared with the analogous reaction of an anionic nucleophile with a neutral electrophile.

The $\text{S}_{\text{N}}2$ reaction profile for $\text{H}_2\text{O} + \text{Bu}^t-\text{OH}_2^+$ *in vacuo* and in PCM water shows a sequence of three steps, each with a transition structure corresponding to internal rotation of a single methyl substituent. The same three rotations also appear in the $\text{S}_{\text{N}}2$ reaction profile for $\text{Cl}^- + \text{Bu}^t-\text{Cl}$, but as distinct stages of a concerted process with a single transition structure; only the second methyl group undergoes internal rotation in the transition vector itself. In view of the current debate as to whether the *tert*-butyl cation actually exists in water,³² these results are intriguing. It would be of interest to carry out a dynamical study of the $\text{H}_2\text{O} + \text{Bu}^t-\text{OH}_2^+$ exchange reaction. The polarized continuum model omits specific hydrogen bonding, which may be of considerable significance in this system. We are presently carrying out hybrid quantum-mechanical/molecular-mechanical calculations with explicit solvent water molecules for this reaction and its homologs.

The AM1/COSMO enthalpy surfaces suggest the existence

of both $\text{S}_{\text{N}}2$ and $\text{S}_{\text{N}}1$ mechanistic pathways for the identity reaction $\text{H}_2\text{O} + \text{R}-\text{OH}_2^+$ with each alkyl group R . Mechanistic change occurs by alteration of the relative energies of the TSs along these competing paths. These surfaces provide no evidence to support alternative possibilities for mechanistic changeover, such as the 'merging' pathway of Doering and Zeiss,²⁸ or a discontinuous jump from one mechanism to another.²⁷ Calculated 2 α -D KIEs are in accord with expectation: values close to unity for reactions involving a tight TS, but large and normal for reactions involving a loose TS. The value predicted for the $\text{S}_{\text{N}}2$ mechanism with $\text{R} = \text{Pr}^i$ has a magnitude that might easily be assigned to an $\text{S}_{\text{N}}1$ mechanism according to the conventional view. A feature of the computational modeling approach to reactivity is the ability to examine experimentally unobserved reaction mechanisms.

Acknowledgements

We thank the EPSRC for support under GR/M40851, and the HEFCE/EPSRC JREI for equipment.

References

- 1 C. K. Ingold, *Structure and Mechanism in Organic Chemistry*, 2nd edn., Cornell University Press, Ithaca, 1969; P. B. D. de la Mare, L. Fowden, E. D. Hughes, C. K. Ingold and J. D. H. Mackie, *J. Chem. Soc.*, 1955, 3200.
- 2 S. Winstein, S. Smith and D. Darwish, *Tetrahedron Lett.*, 1959, 24.
- 3 D. Samuel and B. L. Silver, *Adv. Phys. Org. Chem.*, 1965, 3, 123.
- 4 R. A. McClelland, *Can. J. Chem.*, 1980, **58**, 393.
- 5 E. Uggerud and L. Bache-Andreassen, *Chem. Eur. J.*, 1999, **5**, 1917.
- 6 Gaussian 98, Revision A.6: M. J. Frisch, G. W. Trucks, H. B. Schlegel, G. E. Scuseria, M. A. Robb, J. R. Cheeseman, V. G. Zakrzewski, J. A. Montgomery, Jr., R. E. Stratmann, J. C. Burant, S. Dapprich, J. M. Millam, A. D. Daniels, K. N. Kudin, M. C. Strain, O. Farkas, J. Tomasi, V. Barone, M. Cossi, R. Cammi, B. Mennucci, C. Pomelli, C. Adamo, S. Clifford, J. Ochterski, G. A. Petersson, P. Y. Ayala, Q. Cui, K. Morokuma, D. K. Malick, A. D. Rabuck, K. Raghavachari, J. B. Foresman, J. Cioslowski, J. V. Ortiz, B. B. Stefanov, G. Liu, A. Liashenko, P. Piskorz, I. Komaromi, R. Gomperts, R. L. Martin, D. J. Fox, T. Keith, M. A. Al-Laham,

- C. Y. Peng, A. Nanayakkara, C. Gonzalez, M. Challacombe, P. M. W. Gill, B. Johnson, W. Chen, M. W. Wong, J. L. Andres, M. Head-Gordon, E. S. Replogle and J. A. Pople, Gaussian, Inc., Pittsburgh, PA, 1998.
- 7 S. Miertuš, E. Scrocco and J. Tomasi, *Chem. Phys.*, 1981, **55**, 117; R. Cammi and J. Tomasi, *J. Chem. Phys.*, 1994, **100**, 7495.
- 8 MOPAC93, J. J. P. Stewart and Fujitsu Limited, Tokyo, 1993.
- 9 A. Klamt and G. Schüürmann, *J. Chem. Soc., Perkin Trans. 2*, 1993, 799.
- 10 I. H. Williams, *Chem. Phys. Lett.*, 1982, **88**, 462; I. H. Williams, *THEOCHEM*, 1983, **94**, 275.
- 11 L. Melander and W. H. Saunders, *Reaction Rates of Isotopic Molecules*, Wiley, New York, 1980.
- 12 L. Pauling, *J. Am. Chem. Soc.*, 1947, **69**, 542.
- 13 J. Wilkie and I. H. Williams, *J. Chem. Soc., Perkin Trans. 2*, 1995, 1559.
- 14 V. Moliner and I. H. Williams, *J. Am. Chem. Soc.*, 2000, **122**, 10895.
- 15 W. J. Albery and M. M. Kreevoy, *Adv. Phys. Org. Chem.*, 1978, **15**, 87.
- 16 F. Jensen, *Chem. Phys. Lett.*, 1992, **196**, 368.
- 17 C. Li, P. Ross, J. E. Szulejko and T. B. McMahon, *J. Am. Chem. Soc.*, 1996, **118**, 9360.
- 18 M. Wladkowski and J. I. Brauman, *J. Phys. Chem.*, 1993, **97**, 13158.
- 19 L. Deng, V. Branchadell and T. Ziegler, *J. Am. Chem. Soc.*, 1994, **116**, 10645; T. N. Truong and E. V. Stefanovitch, *J. Phys. Chem.*, 1995, **99**, 14700.
- 20 M. N. Glukhovtsev, A. Pross and L. Radom, *J. Am. Chem. Soc.*, 1995, **117**, 2024.
- 21 M. Cossi, C. Adamo and V. Barone, *Chem. Phys. Lett.*, 1998, **297**, 1.
- 22 G. D. Ruggiero, PhD Thesis, University of Bath, 1999.
- 23 B. L. Knier and W. P. Jencks, *J. Am. Chem. Soc.*, 1980, **102**, 6789; G.-A. Craze and A. J. Kirby, *J. Chem. Soc., Perkin Trans. 2*, 1978, 357.
- 24 A. Streitwieser, G. S.-C. Choy and F. Abu-Hasanayn, *J. Am. Chem. Soc.*, 1997, **119**, 5013.
- 25 E. D. Hughes, C. K. Ingold and U. G. Shapiro, *J. Chem. Soc.*, 1936, 225.
- 26 J. R. Murdoch, *THEOCHEM*, 1988, **40**, 447; R. B. Hammond and I. H. Williams, *J. Chem. Soc., Perkin Trans. 2*, 1989, 59.
- 27 W. P. Jencks, *Acc. Chem. Res.*, 1976, **9**, 425; W. P. Jencks, *Acc. Chem. Res.*, 1980, **13**, 161.
- 28 W. E. Doering and H. H. Zeiss, *J. Am. Chem. Soc.*, 1953, **75**, 4733.
- 29 J. A. Barnes, J. Wilkie and I. H. Williams, *J. Chem. Soc., Faraday Trans.*, 1994, **90**, 1709.
- 30 M. H. Abraham, *J. Chem. Soc., Perkin Trans. 2*, 1973, 1893.
- 31 J. A. Barnes and I. H. Williams, *J. Chem. Soc., Chem. Commun.*, 1993, 1286.
- 32 M. M. Toteva and J. P. Richard, *J. Am. Chem. Soc.*, 1996, **118**, 11434; Q. S. Meng and A. Thibblin, *J. Chem. Soc., Perkin Trans. 2*, 1999, 1397.